An *in situ* study of the *t*-butyllithium initiated polymerization of butadiene in *d*-heptane via small angle neutron scattering and ^{1}H-NMR

A. Z. Niu, J. Stellbrink,[a] J. Allgaier, L. Willner, A. Radulescu, and D. Richter
Institut für Festkörperforschung, Forschungszentrum Jülich GmbH, 52425 Jülich, Germany

B. W. Koenig
Institut für Biologische Informationsverarbeitung 2, Forschungszentrum Jülich GmbH, 52425 Jülich, Germany and Institut für Physikalische Biologie, Heinrigh-Heine Universität 40228 Düseldorf, Germany

R. P. May
Institute Laue-Langevin, 6, rue Jules Horowitz, F-38042 Grenoble Cedex 9, France

L. J. Fetters
School of Chemical and Biomolecular Engineering, Cornell University, Ithaca, New York 14583-5201

(Received 22 December 2004; accepted 11 January 2005; published online 5 April 2005)

We present a combined ^{1}H-NMR and small angle neutron scattering *in situ* study of the anionic polymerization of butadiene using *t*-butyllithium as the initiator. Both initiation and propagation phases were explored. This combined approach allows the structural and kinetic characteristics to be accessed and cross compared. The use of the D22 instrument (ILL Grenoble) permits the attainment of $Q \approx 2 \times 10^{-3}$ Å. This, in turn, led to the identification of coexisting large-scale and smaller aggregates during all stages of the polymerization. The smaller aggregates contain most of the reacted monomers. Their structure changes from high functionality wormlike chains at early stages of the reaction to starlike aggregates where the crossover occurs at a degree of polymerization of ≈40. The initiation event involved these small, high functionality (≈120) aggregates that apparently consisted of cross-associated *t*-butyllithium with the newly formed allylic-lithium head groups. As the initiation event progressed the initiation rate increased while the functionality of these small aggregates decreased and their size increased. Propagation, in the absence of initiation, was found to have a rate constant that was molecular weight dependent. At ~11 kg/mol the measured polymerization rate was found to increase while no further structural changes were seen. © *2005 American Institute of Physics*. [DOI: 10.1063/1.1866092]

I. INTRODUCTION

A. Head-group aggregation

Organolithium compounds are the most common initiators in commercial anionic polymerizations. Aggregation phenomena are of substantial relevance for this important polymerization family. The aggregation of these species, when converted to the head groups derived from dienes or styrene (the initiation step) and the subsequent propagation event, would be expected to influence kinetic behavior and rates. These compounds spontaneously self-assemble in hydrocarbon and ethereal solvents. This naturally occurs as a consequence of the lipophobic identity of the semi-ionic head groups and their lipophilic tails. These species can hence qualify as surfactants. In hydrocarbons ethyllithium, propyllithium, and the butyllithium isomers yield association states[1] of 4 or 6. The aggregation behavior of 2-methylbutyllithium, while showing us an aggregation state of 6 for concentrations $>0.4M$ in pentane at 18 °C, also demonstrated the influence of temperature and concentration upon the association state. Average association states of ~2.6–7.6 were observed.[2] Hydrocarbon insoluble species such as the benzyllithium and allyllithium structures assume stacked arrays in the solid state[3] when a Lewis base is present.

The anionic polymerization kinetics and mechanism are complicated by the aforementioned association phenomena. Here we give a short summary of the commonly accepted mechanism.[1,4–8] The mechanism for living anionic polymerization consists of two primary reaction steps:
(1) initiation,

$$\mathrm{BuLi} + M \xrightarrow{k_i} \mathrm{Bu} - M\mathrm{Li}; \tag{1}$$

(2) propagation,

$$\mathrm{Bu} - (M)_{n-1} - M\mathrm{Li} + M \xrightarrow{k_p} \mathrm{Bu} - (M)_n - M\mathrm{Li}. \tag{2}$$

Here BuLi denotes the initiating organolithium compound, M is the monomer unit, n is the number of monomers incorporated in the living chain, $n+1=D_p$ is the degree of polymerization, and k_i and k_p the rate constants for the initiation and propagation steps, respectively. Under controlled polymerization conditions these systems are free of spontaneous termination events.

Initiation and propagation both have their own preequilibrium with respect to association, with n_{agg} the aggregation number of the corresponding aggregating species with $K_{i,D}$

[a]Author to whom correspondence should be addressed. Electronic mail: j.stellbrink@fz-juelich.de

$=[K_{i,A}]^{-1}$ and $K_{p,D}=[K_{p,A}]^{-1}$ the equilibrium constants for dissociation and aggregation for the initiator and the growing chain:

$$[(\mathrm{BuLi})_{n_{agg(ini)}} \overset{K_{i,D}}{\leftrightarrow} n_{agg(ini)}\ \mathrm{BuLi}], \tag{3}$$

$$[(\mathrm{Bu}-(M)_n-M\mathrm{Li})_{n_{agg(prop)}} \overset{K_{p,D}}{\leftrightarrow} n_{agg(prop)}\ \mathrm{Bu}-(M)_n-M\mathrm{Li}]. \tag{4}$$

The following assumptions are then in place: (i) The equilibrium events are shifted mainly towards the aggregated species, i.e., $K_{i,D} \ll 1$ and $K_{p,D} \ll 1$, and (ii) The only reactive species is the nonaggregated one.

The commonly accepted textbook rate equations for initiation and propagation read as follows:

$$\frac{d[I]}{dt} = -k_i[M][I]^{1/n_{agg(ini)}}, \tag{5}$$

$$\frac{d[M]}{dt} = -k_p[M][I]^{1/n_{agg(prop)}}. \tag{6}$$

Here the square brackets denote the concentration of the corresponding components, that is, the reaction order with respect to initiator concentration directly reflects the aggregation state of the corresponding organolithium compound. This scenario is simplified in that it ignores the role of cross-aggregated structures formed from the initiator and the newly formed styryllithium or dienyllithium head groups during the period where initiation and propagation are occurring simultaneously.

These respective notions were motivated by the 1960 paper[9] regarding the reaction of *n*-butyllithium with styrene in benzene. This system was found to exhibit (30 °C) $\sim 1/6$ order for initiation and $\sim 1/2$ order for the propagation event. Subsequently, kinetic orders of 0.62–0.91 for the propagation event of styrenic monomers have been reported in benzene and toluene[10–14] while an order of $\sim 1/2$ was found for styrene/cyclohexane[15,16] at 40 °C.

The mechanism was extended to dienes via the propagation kinetic work of Worsfold, Bywater, and Johnson.[15–18] Their reported kinetic orders were 1/4 for isoprene[15,17,18] and $\sim 1/6$ for butadiene.[16] In 1972 the butadiene value was altered[19] to 1/4. These cyclohexane[16,17] and benzene[18] based diene kinetic data sets were subsequently shown[20] to share the common experimental propagation reaction order of $0.19_4(\pm 0.017)$.

The postpolymerization aggregation states of these living polymers have been investigated by concentrated solution viscosity,[21–25] bulk viscosity,[26] static light scattering,[19,25,27] intrinsic viscosity.[27] dynamic light scattering,[28] and small angle neutron scattering[29–32] (SANS) measurements. Viscosity measurements are limited in the amount of direct structural information obtainable for the case where nonlinear aggregates are present. Conventional static multiangle and low angle laser light scattering for isoprenyl lithium and butadienyl lithium head groups led to apparent association states of two and four.[19,25,27] The concentrated solution viscosity method revealed[21–25] a common aggregation state (n_{agg}) of 2. This was in conflict with the mechanistic requirement that the sole state of association for the dienyllithium species is the tetramer.[4,5,7,8] In addition, rheological and ^{7}Li-NMR experiments[33] on the lifetime of the aggregates show that the vicosimetric method accurately reflects the limiting aggregate state of 2 for high molecular weight chains.

SANS (Refs. 28–32) and dynamic light scattering[28] have revealed the presence of large-scale objects, $R_g \approx 10^3$ Å,[34] for low molecular weight poly(butadienyl)lithium. Bywater[35] challenged the existence of these large-scale structures. SANS data demonstrated[29] that the styryllithium aggregates in benzene are a mixture of large-scale objects, starlike structures, and dimers.

For a detailed understanding of any chemical reaction two types of information are prerequisite. First the reaction kinetics that are obtained from the time dependence of all reactant concentrations results in the underlying rate equation. Second the reaction mechanism, which is obtained from structural information of reactants, products, and in particular (if possible), intermediate species. Only the combination of all will enable us to fully understand and control a chemical reaction. A comprehensive simultaneous experimental investigation that covers both kinetic and structural aspects of anionic polymerization has not yet, until now, been performed. On the other hand theoretical work concerning the influence of chain length on the association phenomena is found in the literature.[36] This work utilizes the joint techniques of simultaneous *in situ* SANS and ^{1}H-NMR measurements. The former yields structural information about the aggregates as a function of time while ^{1}H-NMR provides insight into the concurrent initiation and propagation events via the simultaneous measure of initiator and monomer concentrations. The polymerization of butadiene in *n*-heptane initiated by *t*-butyllithium was examined.

II. EXPERIMENT

A. General procedures

The monomer, solvent, and initiator purifications were carried out on a high vacuum line. The general techniques have been described elsewhere.[37] Butadiene (Fluka, >99.5%) and deuterated *n*-heptane (Chemotrade, 99 atom%*d*) were degassed, stirred over CaH_2 (Ref. 38) for two weeks and then distilled into flasks with fresh sodium mirrors. The deuterated *n*-heptane was then stirred for three days over the sodium mirror at room temperature while butadiene was stirred for ~6 h at −40 °C. The final drying step was carried out with solvent free *n*-butyllithium. Butadiene was stirred for 20 min at −10 °C and *n*-heptane overnight at room temperature. The drying procedures with CaH_2 and sodium were used to minimize the content of protic impurities in the reagents. Direct contact of the unpurified monomer and solvent with butyllithium or dibutylmagnesium would generate butane. The ^{1}H-NMR signals of the butanes are expected in the same area where signals of initiator/initiating unit appear and would make the analysis of the initiating process more difficult. *t*-Butyllithium (Aldrich, 1.7*M* solution in pentane) was sublimed under high vacuum conditions

TABLE I. Characteristics of the polymerization reaction and the obtained polybutadienes from the *in situ* measurements.

	$[M]_0$ (mol/L)	$[t\text{-BuLi}]_0$ (mol/L)	M_n(kg/mol)			M_w(kg/mol)		M_w/M_n	R_g(nm)	A_2 (cm^3 mol/g^2)
			Calculated[a]	NMR[b]	SEC	SANS	SEC	SEC	SANS	SANS
SANS sample	0.80	1.37×10^{-3}	31.5	–	32.8	35.6	35.4	1.08	9.0	2.88×10^{-3}
NMR sample	0.81	1.34×10^{-3}	32.6	32.6	32.0	–	34.6	1.07	8.8	–

[a]$M_n = 54[M]_0/[t\text{-BuLi}]_0$.
[b]Final measurement.

after having removed the solvent. It was then redissolved in *n*-hexane that was previously dried over *n*-butyllithium. Hydrolyzing an aliquot with distilled water and titrating the LiOH formed with standard hydrochloric acid determined the *t*-butyllithium concentration. From another aliquot the hexane was removed and replaced by *d*-heptane. As this procedure was carried out using flasks equipped with Young® stopcocks, the weights of hexane and *n*-heptane could be precisely measured using an analytical balance. Thus the *t*-butyllithium concentration in *n*-heptane could be calculated with good precision.

The polymerization reactions were carried out directly in sealed ^{1}H-NMR tubes and SANS quartz cells. The tubes and cells were equipped with Young® stopcocks and were flamed under high vacuum conditions. They were then transferred into the glove box (MBraun, Unilab®, <0.1 ppm O_2 and <1 ppm H_2O) and the initiator/*n*-heptane solution was transferred to the reactors via a microliter syringe. The polymerization reactors were transferred back to the vacuum line, cooled, and the argon was removed. Butadiene and additional *n*-heptane were distilled from *n*-butyllithium solutions into small flasks equipped with Young® stopcocks. Again, this allowed the weights of the ingredients to be precisely measured. Monomer and solvent were then distilled quantitatively from the small flasks into the tubes and cells. The NMR cells were sealed off at liquid nitrogen temperature and the SANS cells were sealed off at −78 °C. The higher temperature in case of the SANS cells was necessary to prevent the glass from cracking during the warm up procedure. The samples were stored at −78 °C until the measurements commenced.

Polymerization reactions were carried out in the NMR instrument and the neutron beam at 8 °C (±0.7 °C) continuously monitoring the reaction. This temperature was chosen to diminish reactivity to an extent that the overall reaction time was at least several days. By means of this measure it was possible to follow in detail the initiation and propagation events.

The start of the scattering measurements was synchronized with the commencement of the polymerization event. We initially collected data in 5 min slices and found that under these experimental conditions the polymerization is quite slow. Therefore we relaxed our temporal resolution and averaged at each case 4 of these 5 min runs to improve statistics and to align our SANS experiments with the *in situ* ^{1}H-NMR. Furthermore we used the data collected during the first 20 min of the polymerization to correct all further data with this "background run." That is, the scattering intensities shown in the following sections unambiguously result from the polymerization event with no contribution from background scattering.

When the polymerization was finished the cells were opened in the glove box and terminated with degassed methanol. The solvents were evaporated and the polymers dried. The samples were characterized via size exclusion chromatography (SEC) coupled with on-line light scattering detection. The SEC solvent was tetrahydrofurane (THF) at 30 °C. The characterization results of the terminated polymers are shown in Table I. Besides the reaction temperature the design of the SANS cells and the NMR tubes is important. In the initial experiments it was found that if conventional NMR tubes were used 20% of the butadiene was located in the head room which accounted for 75% of the tube volume. In order to have similar conditions in the NMR tube and the SANS cell and to exclude influences of gas diffusion processes on reaction kinetics the tubes and cells were redesigned. They contained a capillary on top which allowed their near quantitative filling followed by the sealing procedure without warming the reagents. The details are given elsewhere.[31,32]

B. ^{1}H-NMR experiments

Proton NMR spectra were recorded at a Larmor frequency of 600.14 MHz on a Bruker DMX600 using a 5 mm high resolution triple resonance probe optimized for proton observation. The free induction decay was recorded immediately after a nonselective 90° pulse (7 μs) with a dwell time of 111 μs and 32*k* data points in the time domain. Four transients were added for each spectrum using the CYCLOPS phase cycle to avoid artifacts from quadrature detection. A long prescan delay of 300 s was found to be necessary to ensure complete T_1 relaxation of all signals (a strict requirement for quantitative interpretation of integral peak intensity). An exponential window function was applied prior to Fourier transformation and integration of the frequency domain signals.

Careful optimization of experimental conditions was crucial for the quantitative interpretation of the ^{1}H-NMR spectra. The design of the sample cell, the filling factor of the sealed NMR tube, and the length of the relaxation period required between subsequent scans were found to be critical. The T_1 relaxation times of the monomer peaks were determined to be (40±5) s at 8 °C. Spin-lattice relaxation times are significantly shorter for the polymer peaks and decreased with the length of the polymer chain as expected for rapidly tumbling molecules in solution. The most likely explanation for the rather long T_1 values of the solute is solvent deutera-

tion. Nuclear dipole-dipole interaction is a very important relaxation mechanism for protons. The interaction with other nearby protons is particularly efficient due to the extraordinary high gyromagnetic ratio γ of protons. Replacing solvent protons with low γ deuterons will increase T_1 of the solute. Paramagnetic impurities, e.g., molecular oxygen, provide another efficient source of T_1 relaxation. However, trace amounts of oxygen were removed during the purification and degassing procedures. For the quantitative ^{1}H-NMR experiments a prescan delay of 300 s was used. Further increasing the delay to 1000 s did not change the integral intensity of any relevant peaks in the spectrum by more than 1%.

The deuteration degree of *n*-heptane was determined in separate experiments by measuring mixtures of known amounts of *n*-heptane and 1,1,2,2-tetrabromoethane. From the intensity ratio of the tetrabromoethane signal at 6.1 ppm and the heptane signals the deuteration degree could be calculated (99.0%). Knowing the weights of initiator, monomer, and solvent in the polymerization tube, it was possible to calculate initial monomer and initiator concentrations for the polymerization experiment.

Furthermore the possible effect of initiator impurities was studied by ^{1}H-NMR in deuterated benzene as the solvent. The benzene (Aldrich, 99.6 atom%*d*) was purified in the same manner as described for the heptane. Lithium *t*-butoxide (Aldrich, 1*M* solution in hexane) and isobutane (Fluka) are potential impurities resulting from *t*-butyllithium. Both could influence the ^{1}H-NMR analysis. Samples of *t*-butyllithium, lithium *t*-butoxide, isobutane, and a mixed sample of *t*-butyllithium and lithium *t*-butoxide in *d*-benzene were prepared as described for the polymerization sample.

Lithium-alkoxide cannot be readily separated from the *t*-butyllithium via vacuum sublimation. This impurity could be formed during sample preparation (or earlier) via reaction with oxygen. As alkoxides (and possibly hydroxides) influence polymerization rates and form cross aggregates with the butyllithium isomers[4,39–43] the purity of the *t*-butyllithium used in the experiment was investigated in separate ^{1}H-NMR experiments. If *n*-heptane is used as solvent, the butoxide and the isobutane signals are partially hidden by the solvent signals. For this reason the purity check was carried out in benzene. Three samples containing *t*-butyllithium, lithium *t*-butoxide, and isobutane were prepared at a concentration level comparable to the *t*-butyllithium concentration in the polymerization experiment. In benzene *t*-butyllithium gives a signal at 0.97 ppm whereas the signal for the *t*-butoxide appears at 1.27 ppm and the signals for isobutane appear at 0.87 ppm (doublet, 9 protons) and 1.63 ppm (multiplet, 1 proton). In the sample containing *t*-butyllithium the butoxide and isobutane were not detected. As butyllithium and lithium butoxide form cross aggregates[39–43] it is possible that the chemical shifts of the pure substances change if both substances are present. For this reason a mixed *t*-butyllithium/lithium *t*-butoxide sample was prepared in a molar ratio of $\approx 2:1$. In the spectrum the signals from *t*-butyllithium disappeared while the lithium *t*-butoxide signal was reduced to $\approx$10% of the expected intensity. Instead of that a multitude of signals appeared between 1.20 and 1.60 ppm. Most likely these signals come from mixed aggregates having different aggregation numbers and/or *t*-butyllithium-lithium *t*-butoxide compositions. As the *t*-butyllithium sample also did not show the signals between 1.20 and 1.60 ppm it was concluded that the initiator system was free of lithium *t*-butoxide and lithium hydroxide. This conclusion is supported by the molecular weight measurements of the polymerized NMR and SANS samples. The measured molecular weights are in good agreement with the calculated values from sample preparation parameters; see Table I. The initiator solutions were kept at −10 °C. The solutions remained clear and colorless.

C. SANS experiments

The experimental quantity observed in a SANS experiment is the intensity in terms of the macroscopic cross section $[d\Sigma/\Omega](\mathrm{Q})$. Assuming that the growing polymer chains form aggregates with a mean aggregation number n_{agg}, $[d\Sigma/\Omega]$ as a function of reaction time, and the scattering vector Q are given by

$$\frac{d\Sigma}{d\Omega}(Q,t) = \frac{\Delta\rho^2}{N_a}\phi_p(t)n_{agg}(t)V_w(t)P_{agg}(Q,t). \tag{7}$$

Here, polymer concentration is given in terms of ϕ_{p} which denotes the polymer volume fraction and $V_{\mathrm{w}}=M_{\mathrm{w}}/\rho$ is the corresponding weight average molecular volume or weight of the growing chains, ρ is the polymer density. $P_{\mathrm{agg}}(Q,t)$ is the form factor of the aggregated species and contains the structural information. $\Delta\rho$ is the scattering contrast:

$$\Delta\rho = \left[\frac{\Sigma b_s}{v_s} - \frac{\Sigma b_{mon}}{v_{mon}}\right]. \tag{8}$$

The ratio $\Sigma b_s/v_s$ is the scattering length density of the solvent with b_s the scattering lengths of the atoms forming the solvent molecule and v_s the corresponding volume. $\Sigma b_{mon}/v_{mon}$ is the corresponding quantity for the repeat unit and N_{a} the Avagadro number. Finally, $Q=[4\pi/\lambda]\sin\Theta/2$ is the scattering vector with λ the neutron wavelength and Θ the scattering angle. For starlike aggregates Benoit[44] has given a form factor assuming Gaussian conformation of the arms. This is the only Q-dependent variable in Eq. (7):

$$P_{star}(Q) = \frac{2}{f\,Q^4R_{g,arm}^4}\left[Q^2R_{g,arm}^2 - (1-e^{-Q^2R_{g,arm}^2}) + \frac{f-1}{2}(1-e^{-Q^2R_{g,arm}^2})^2\right]. \tag{9}$$

Here f is the star polymer functionality and $R_{\mathrm{g,arm}}$ the radius of gyration of the constituting linear polymer chains (the "arms"). In our case $f=n_{\mathrm{agg}}$ and $R_{\mathrm{g,arm}}$ is related to M_{w} of the growing polymer chain by the scaling relation $R_{\mathrm{g,arm}}\sim M_{\mathrm{w}}^{\nu}$, with ν the Flory exponent. [For simplicity we have neglected the concentration dependence, i.e., the second virial coefficient, of $d\Sigma/d\Omega(Q,t)$.] In a previous publication[28] we have shown that under the assumptions below all time dependent quantities in Eq. (9) can be reduced to one parameter. Thus, the number density of reacted monomers, $N_{\mathrm{p}}(t)$ can be calculated from the observed forward scattering $\mathrm{I}(\mathrm{Q}=0,t)$. The assumptions are the following.

(i) The number of living chains is time independent and equal to the initiator concentration, i.e., the initiation period is over.
(ii) All chain head-groups participate in all aggregates with a time independent aggregation number.
In this case SANS data alone will yield direct access to the kinetics of reaction.

If our studies include systems with different types of aggregates or aggregation numbers that change with time we then need additional quantitative information to unambiguously interpret the SANS data. The needed information can be independently obtained from time resolved ^{1}H-NMR experiments, which gives us directly $[I(t)]$, $[M(t)]$, and $[P(t)]$, from which we further can calculate the degree of polymerization $D_P(t)$ and $M_n(t)$ the number average molecular weight. If we now use these data to analyze our SANS data we can directly access the aggregation number as a function of time for all phases of the polymerization.

Q has the dimensions of a reciprocal length and can therefore be regarded as an "inverse meter stick." For SANS experiments typically performed with different settings, i.e., different sample-to-detector distances and collimation lengths, a Q range of nearly 2.5 orders of magnitude can be achieved, $1\times10^{-3}\leqslant Q\leqslant 0.2$ Å^{-1}. This corresponds to a spatial resolution 5 Å$\leqslant D=1/Q\leqslant$1000 Å. Changing detector and collimation settings may require several minutes. This can substantially reduce the temporal resolution of a time-resolved experiment. For this reason a compromise between the accessible Q range and time resolution is required.

The SANS measurements were performed at the KWS2 instrument at the Forschungszentrum Jülich (Germany), and the D22 instrument at the Institute Laue-Langevin-Grenoble (France). For KWS2 we chose a sample-to-detector distance $D=8$ m and a collimation length $L=8$ m using a neutron wavelength $\lambda=7.3$ Å with a wavelength spread $\Delta\lambda/\lambda=10\%$. This covers a Q range of $6.9\times10^{-3}\leqslant Q\leqslant 2.7\times10^{-2}$ Å^{-1}. The D22 experiments were performed with $D=18$ m, $L=17.6$ m, and $\lambda=8$ Å, $\Delta\lambda/\lambda=10\%$. In addition, at D22, we measured with an off-centred detector position, $D_{offset}=390$ mm, which enlarges the Q range to $Q_{max}/Q_{min}\approx 20$, i.e., $2.2\times10^{-3}\leqslant Q\leqslant 4.2\times10^{-2}$ Å^{-1}.

For polymers in dilute solution, Eq. (7) is given by

$$\left(\frac{d\Sigma}{d\Omega}\right)_{macr.}=\frac{\Delta\rho^2}{N_a}\frac{\phi\,(1-\phi)}{\left[\dfrac{1}{n_{agg}V_w\,P(Q)}+2A_2\,\phi\right]}. \tag{10}$$

Here, $P(Q)$ is the form factor and A_2 the second virial coefficient.

To achieve maximum contrast and minimum incoherent background resulting from protonated material, we investigated the polymerization of *h*-butadiene initiated by *h*-*t*-butyllithium in *d*-heptane ($\rho_{h\text{-butadiene}}=4.12\times10^{+9}$ cm^{-2}, $\rho_{d\text{-heptane}}=6.26\times10^{+10}$ cm^{-2}, $\Delta\rho=5.85\times10^{+10}$ cm^{-2}; $\rho_{h\text{-buli}}=-8.44\times10^{+9}$ cm^{-2}, $\Delta\rho=-7.09\times10^{+10}$ cm^{-2}). Because all b_i terms are well defined and tabulated properties of the corresponding nucleus the SANS data are obtained on an absolute scale and can be interpreted quantitatively without any ambiguity.

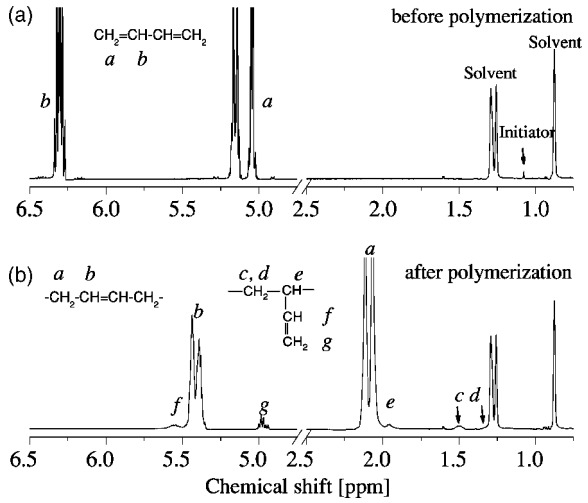

FIG. 1. ^{1}H-NMR spectra before and after polymerization (full ppm range).

In general, all azimuthally averaged data were corrected for empty cell scattering and then normalized to the absolute scattering cross section (cm^{-1}) using a 1 mm water standard. Contributions due to incoherent background and solvent scattering were subtracted from all data sets before analysis. A useful presentation of the theory and practice of SANS is available from Higgins and Benoit.[45]

III. RESULTS

For the polymerization study, the combination of ^{1}H-NMR and SANS was chosen. Using time resolved ^{1}H-NMR we obtained quantitative information concerning initiator concentration $[I(t)]$, monomer concentration $[M(t)]$, polymer concentration $[P(t)]=[M(t=0)]-[M(t)]$, and degree of polymerization $D_p(t)$ of the growing chains as a function of time and conversion. Previous UV-visible spectrometry based studies were incapable of these multiple and simultaneous measurements. Time-resolved SANS on the other hand provides us structural information on the mesoscopic and microscopic length scales, e.g., the radius of gyration $R_g(t)$ of intermediate aggregates and quantitative information concerning their molecular weight or scattering volume. This enables us to simultaneously cross check kinetics (^{1}H-NMR) with aggregate structural data (SANS) thus rendering this combination of experimental techniques especially appealing. The individual results of both experiments will be separately presented in the following two sections before we show the results derived from a combination of ^{1}H-NMR and SANS data.

A. ^{1}H-NMR results

Figure 1 shows the ^{1}H-NMR spectra before and after polymerization. All signals can be assigned to the detailed chemical microstructure of the individual components. The two monomer signals arise at ~6.3 ppm (CH) and at ~5.1 ppm (CH_2). The polymer signals are found at ~5.4 and ~2.1 ppm for the 1,4 structure, and at ~5.5, ~5.0, ~1.9, and ~1.5 ppm for the 1,2 structure. The weak initiator signal at 1.07 ppm is surrounded by two strong signals arising from the small fraction of residual protonated solvent.

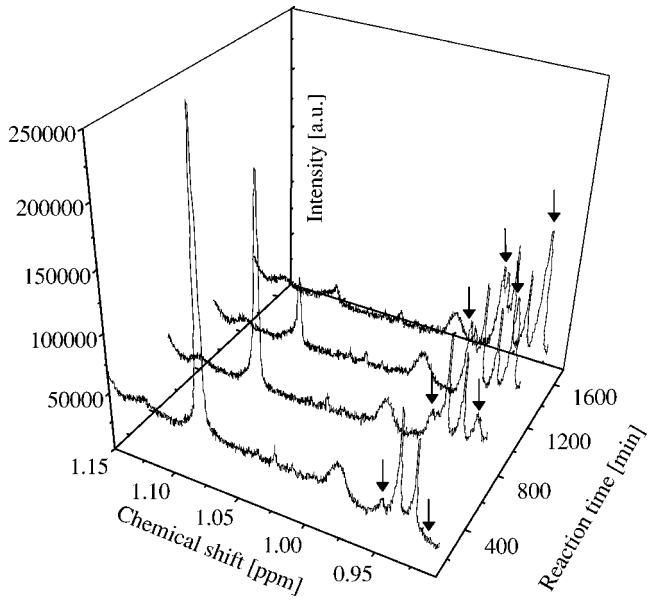

FIG. 2. ^{1}H-NMR spectra of the reacted initiator signals (0.90–1.15 ppm) during initiation. The arrows pin point the initiator signals. The sharp signal at 1.07 ppm originates from the unreacted initiator.

Figure 2 enlarges the area between 0.90–1.15 ppm during the initiation period. The *t*-butyllithium peak is a sharp signal located at 1.07 ppm before polymerization and moves to 0.92 and 0.94 ppm after initiation.

During the polymerization the polymer peaks increase whereas monomer peaks and initiator peak decrease with reaction time (t). For a quantitative analysis of the ^{1}H-NMR spectra it is evident that there exist well-separated peaks that can be unambiguously integrated without any effect from overlap with neighboring peaks. In addition, the numbers of protons correlated with the different signals have to be taken into account. For the comparison of spectra recorded at different reaction times we normalized all signals using the constant solvent peak at 0.85 ppm. Thus, we choose the vinyl peak at ~6.3 ppm for the monomer and the methylene peaks at ~2.1 and ~1.5 ppm for the polymer to calculate our primary quantities of monomer concentration $[M(t)]$ and polymer concentration $[P(t)]$. The initiator concentration $[I(t)]$ is calculated using only the sharp initiator peak at 1.07 ppm. The time dependence of monomer and initiator concentration, normalized to their initial values $[M(t=0)]$ and $[I(t=0)]$, is shown in Fig. 3. In this figure only data encompassing the initiation event are shown. The initiation reaction starts very slowly and then gradually accelerates with concurrent initiator consumption. After ≈24 h no remaining initiator signal is detectable and the initiation period is finished. During this time (where initiation and propagation are running in parallel) a substantial amount of monomer consumption, ≈10%, occurs.

Figures 4(a) and 4(b) show the time dependence of the normalized monomer concentration during the entire polymerization period of ≈14 days. In this period the sample was not investigated continuously by ^{1}H-NMR. During and between these individual runs the polymerizing sample was strictly thermostated at 8 °C in order not to bias the polymerization kinetics. Figure 4(b) enlarges the initiation period. The relations for monomer consumption are given in the following four equations. They represent the monomer consumption during the interval of dual initiation and propagation and the subsequent period where butadiene is solely consumed by propagation. After an initial induction period of ~280 min [Fig. 4(b)], where no conversion of monomer can be detected, four time dependent regions evolve:

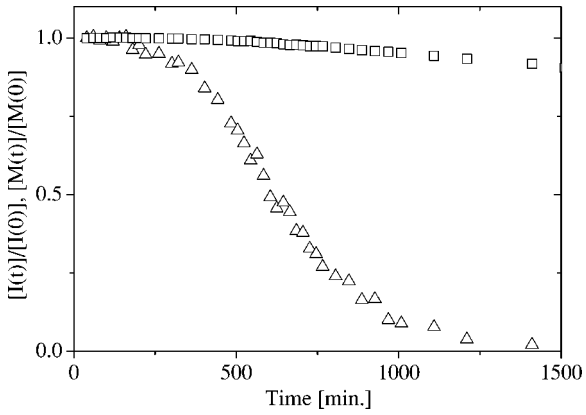

FIG. 3. Time dependence of (Δ, initiator; □, monomer) normalized initiator $[I]/[I]_0$ and monomer concentrations $[M]/[M]_0$ calculated from the *in situ* ^{1}H-NMR spectra as a function of the reaction time (t) during the initiation period.

$$[M]_t/[M]_0 = \exp[-(3.72x10^{-5} \pm 2.0x10^{-6})t] \quad \text{for } 280 < t < 544 \text{ min}, \tag{11a}$$

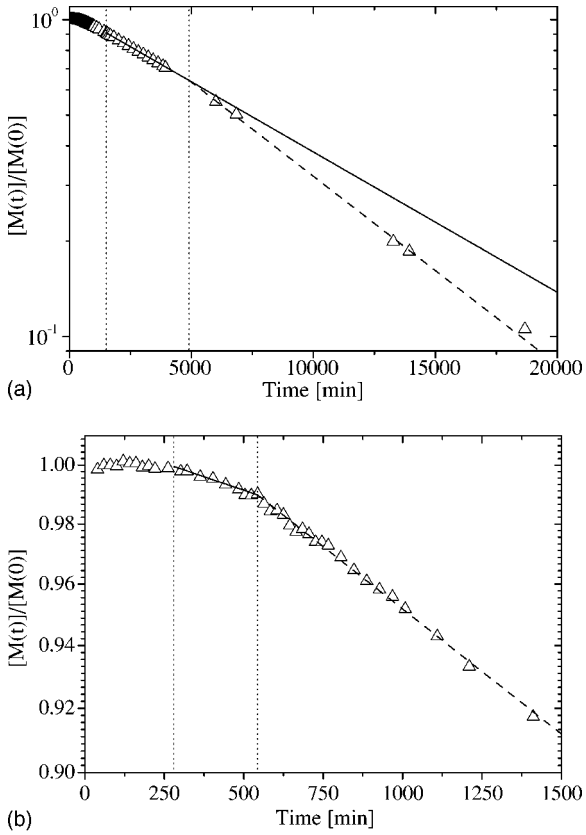

FIG. 4. Time dependence of normalized monomer concentration $[M]/[M]_0$ vs reaction time (t). (a) For the full polymerization period (log-linear plot). (b) The initiation period (log-linear plot). Lines: linear regimes [see Eqs. (11a)–(11d)].

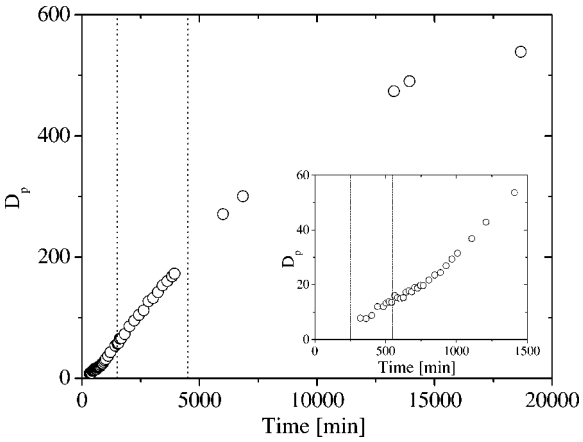

FIG. 5. Time dependence of polymerization degree D_p vs reaction time (t) calculated from the *in situ* ^{1}H-NMR spectra. Inset: Magnification of the initiation period.

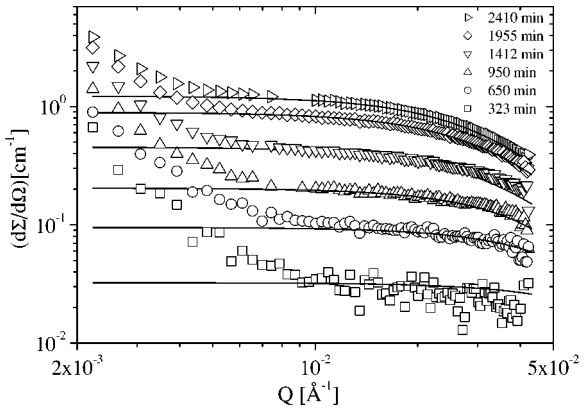

FIG. 6. SANS scattering profiles of living anionic polymerization system (scattering cross section in absolute units vs scattering vector Q) as a function of reaction time (t). Solid lines: Fits from Guinier form factor analysis of the high Q region, Eq. (14).

$$[M]_t/[M]_0 = 1.04\ \exp[-(8.57x10^{-5} \pm 1.2x10^{-6})t] \quad \text{for } 544 < t < 1512 \text{ min}, \tag{11b}$$

$$[M]_t/[M]_0 = 1.06\ \exp[-(1.02x10^{-4} \pm 4.5x10^{-6})t] \quad \text{for } 1512 < t < 4900 \text{ min}, \tag{11c}$$

$$[M]_t/[M]_0 = 1.26\ \exp[-(1.37x10^{-4} \pm 3.5x10^{-6})t] \quad \text{for } 4900 < t < 20\,000 \text{ min}. \tag{11d}$$

Equations (11a) and (11b) cover the temporal range where the initiation and propagation events overlap [Fig. 4(b)]. Interestingly, in the regime of initiation as well as in that of propagation two distinct expressions are required to describe the monomer consumption. In both cases the apparent rates of monomer disappearance increases in passing from one stage to the next. We note however that the second regime of initiation and the first regime of pure propagation are hardly different.

In Eqs. (11c) and (11d) the rate of propagation is seen to increase after ~4900 min. At this point the average D_P of the poly(butadienyl) lithium chain is ~200. There are three previous literature reports where chain length influenced head-group reactivity[13,18,46] and the kinetic order.[46] Using these primary quantities we can calculate the conversion, i.e., the fraction of reacted monomer as a function of time,

$$\mathrm{Conv}(t) = \frac{[P(t)]}{([M(t)] + [P(t)])} = \frac{I_{2.1\ \mathrm{ppm}}(t)/4 + I_{1.5\ \mathrm{ppm}}(t)}{I_{6.3\ \mathrm{ppm}}(t)/2 + I_{2.1\ \mathrm{ppm}}(t)/4 + I_{1.5\ \mathrm{ppm}}(t)}. \tag{12}$$

The degree of polymerization $D_p(t)$ of the growing chain is given by

$$D_P(t) = \frac{[P(t)]}{([I(t=0)] - [I(t)])} = \frac{I_{2.1\ \mathrm{ppm}}(t)/4 + I_{1.5\ \mathrm{ppm}}(t)}{(I_{1.07\ \mathrm{ppm}}(t=0) - I_{1.07\ \mathrm{ppm}}(t))/9}. \tag{13}$$

Figure 5 shows the time dependence of D_p for the entire polymerization period. The inset enlarges the initiation period. After the cessation of the initiation step the average D_p of ~56 is found. This corresponds to a number average chain molecular weight of ~3 kg/mol. The M_w/M_n ratios of the polybutadiene samples at complete conversion are <1.1 (Table I).

B. SANS results

Figure 6 shows the scattering profiles as a function of reaction time (t) obtained by the *in situ* SANS experiment, i.e., the macroscopic scattering cross section ($d\Sigma/d\Omega$) in absolute units versus scattering vector Q. This allows the separation of the monomer consumed via initiation from that incorporated in propagation. The SANS data by themselves reveal important facets concerning the aggregation behavior of the polymerizing sample without being biased by a sophisticated data analysis procedure. Hence we will start with a qualitative discussion of the SANS data before we present the quantitative results of the applied data analysis. The Q range investigated can be divided into two well-separated regions that show a different temporal evolution during the polymerization. The borderline between these two regions is located around $Q = 10^{-2}$ Å^{-1}. For $Q \leqslant 10^{-2}$ Å^{-1}, which will be called the low Q region in the following, all scattering profiles at any reaction time are dominated by an initially strong increase of the scattering intensity towards $Q = 0$. During the early stages of the polymerization a power law behavior, $I(Q) \sim Q^{-P}$, expands over the complete low Q region, showing an intensity drop over nearly two orders of magnitude. At later reaction times the power law seems to flatten, an effect that results from the merging with the increasing intensity level in the high Q region. The observed forward scattering in the low Q region is an indication for the presence of large-scale aggregates in the polymerizing sample.

These structures coexist with both lesser aggregates of allylic lithium and *t*-butyllithium until about 1500 min. We must emphasize that no Guinier or Zimm regime is found in the low Q region. A Guinier or Zimm regime which develops for $QR \leqslant 1$, where R is the characteristic length of the scattering particles, would reveal itself by a tendency towards a constant intensity level/plateau in the log-log representation. This means that for all (t) the size of the large-scale aggregates is at least larger than the inverse of the minimum accessible Q value, $Q=2.2\times10^{-3}$ Å^{-1}, i.e., $R_g \geqslant 500$ Å.

In the high Q region, $Q \geqslant 10^{-2}$ Å^{-1}; on the other hand, we found at small reaction times a flat, completely Q-independent intensity level/plateau, typical for a solution of small particles. With increasing reaction time (t) the intensity level increases and finally a distinct Q dependence evolves. The curvature in the high Q region becomes progressively pronounced and shifts towards lower Q values with increasing conversion. This signals an increase in size of the scattering particles. However even for the largest reaction time under study there remains a distinct Guinier or Zimm regime observable in the high Q region. Using the same arguments as above we can conclude that in the high Q region we monitor the formation of a second class of scattering particles with a characteristic size smaller than the minimum Q value, $Q=10^{-2}$ Å^{-1}, of the high Q region, i.e., $R \leqslant 100$ Å. In the following at intermediate times these smaller particles are characterized as starlike aggregates.

By the use of this simple, qualitative interpretation we can conclude that there are (at least) two distinct classes/types of particles present in the polymerizing solution: (a) Large-scale aggregates with $R_g \geqslant 500$ Å and (b) smaller aggregates with $R_g \leqslant 100$ Å. The large-scale aggregates are present at $t \approx 323$ min (Fig. 6) while the smaller aggregates are hardly visible because of the very low degree of initiation and propagation. It is important to recall that during the 0–1500 min period the initiation and propagation reactions are simultaneously occurring.

Prior to a description of the individual steps of our quantitative analysis, we briefly outline the applied general fitting strategy. This serves to guide the reader through the next section where the parametrization of our time-resolved SANS data is given. For a quantitative analysis of our data over the complete experimental Q range we have to overcome several problems of which the two most crucial are the following. (i) At no stage of the polymerization can we observe a distinct Guinier or Zimm regime for the large scale aggregates. This means that we cannot derive a precise value for their forward scattering; $[d\Sigma/d\Omega](Q=0,t)$ and all related quantities and for their characteristic size. We will only obtain estimates (even from the quantitative analysis) for the minimum limits of these parameters. (ii) In the high Q region at early reaction stages the data points are quite noisy due to their low scattering intensity. (We note that this experiment will push any current SANS instrument to its limits; even D22.) Therefore all fit parameters will show rather large error bars in the early polymerization stages.

To overcome this problem and to minimize the uncertainties in the obtained fit parameters, we applied the following sequential fitting procedure.

(1) As a first step we analyzed the high Q region by means of the model free Guinier approach, Eq. (14) (see below), which characterizes the small aggregates.
(2) Using the derived fit parameters we calculated the scattering profile of the starlike aggregates for the whole Q range and subtracted this theoretical curve from the experimental data. Hence, we obtained the residual scattering arising solely from the large scale aggregates.
(3) This residual scattering is then analyzed by linear regression in a double logarithmic representation, which gives us the power law exponent P.

Using the results from the individual fitting of high and low Q region as starting parameters, the whole experimental Q range is finally analyzed by a sum of a Guinier form factor (for the small aggregates) and the form factor recently introduced by Beaucage[47] (for the large scale aggregates; see below). The details of the individual steps of this sequential fitting procedure will be discussed separately in the following paragraphs, starting with the high Q region.

C. Regime of small aggregates

A model free approach can be applied to the high Q region by use of the Guinier equation, which describes the scattering profile for an individual particle of arbitrary shape in the regime $QR \leqslant 1$:

$$\left(\frac{d\Sigma}{d\Omega}(Q,t)\right)_{.} = \left(\frac{d\Sigma}{d\Omega}(Q=0,t)\right)_{.} \exp[-Q^2R_g^2(t)/3]. \qquad (14)$$

Here the characteristic length of the particle is given in terms of its radius of gyration R_g. The second adjustable parameter in the fitting routine is the forward scattering ($d\Sigma/d\Omega(Q=0,t)$), which is the product of volume fraction $\phi(t)$, the contrast factor $\Delta\rho^2/\mathrm{N_A}$, and molecular volume $V_w(t)$ of the scattering particle:

$$\left(\frac{d\Sigma}{d\Omega}(Q=0,t)\right)_{.} = \phi(t)\frac{\Delta\rho^2}{N_A}V_w(t). \qquad (15)$$

At early reaction times, $t \leqslant 600$ min, the assayed values for $R_g(t)$ and the forward scattering exhibit large uncertainties due to the high noise level and the lack of any pronounced Q dependence in the high Q region. For later reaction times the data quality improves and precise values for $[d\Sigma/d\Omega](Q=0,t)$ and $R_g(t)$ can be obtained. A typical example of experimental data and resulting Guinier fit at these polymerization stages is shown in Fig. 7 for $t=443$ min. The temporal evolution of both parameters is shown in Figs. 8(a) and 8(b). We have to emphasize that the derived values for both parameters do not depend on whether the full Q range or only the high Q data are analyzed. Whereas the forward scattering increases continuously approximately proportional to $\sim t^2$, the radius of gyration $R_g(t)$ seems to be constant within experimental errors for the first 1000 min [Fig. 8(b)].

D. Regime of large scale aggregates

Subtraction of the Guinier fit from the experimental data delivers the residual scattering of the large-scale aggregates as shown in Figs. 7 and 9. The power law decay $[d\Sigma/d\Omega]$

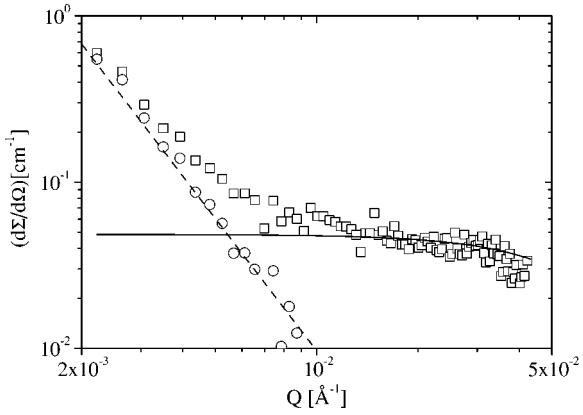

FIG. 7. Typical SANS scattering profile obtained during the initiation period, $t=443$ min., open squares, □ (scattering cross section in absolute units vs scattering vector Q). Open circles, ○—residual power law scattering after subtraction of the Guinier form factor fit (solid line); dashed line—power law fit (linear regression using the log-log plot).

$\sim Q^{-P}$ is clarified substantially by this procedure and can be analyzed in a first approach by linear regression in this log-log representation, revealing a power law exponent P of ≈3.

An enhanced analysis of the low Q region can be done by use of the form factor introduced by Beaucage.[47] His equation can be viewed as a "universal form factor" (for an arbitrary mass fractal) that can also be applied to polymeric systems,

$$d\Sigma/d\Omega(Q) = [\Delta\rho^2/N_A]G\,\exp(-Q^2R^2/3) + B\left(\frac{1}{Q^*}\right)^P, \tag{16}$$

with $Q^*=Q/[\mathrm{erf}(QkR_g/\sqrt{6})]^3$. Here erf is the error function and G and B are amplitudes, which for mass fractals can be related to each other by $B=GP/R_g^P\Gamma(P)$ (polymeric constraint). R is the characteristic size of the scattering particles; P is the fractal dimension of the internal substructure, k an empirical constant is ≅1.06 while Γ is the Gamma function. Equation (16) consists of two terms, one is above the described Guinier term, which in this case describes the large-scale aggregates. As discussed, the Guinier or Zimm regime is missing in the low Q region, so we have to modify Eq. (16) by use of the polymeric constraint and only apply the second term which describes the power law tail. This modified form factor then reads

$$d\Sigma/d\Omega(Q) = GP/R^P\Gamma(P)\left(\frac{1}{Q^*}\right)^P. \tag{17}$$

We note that such a fit cannot really determine aggregate

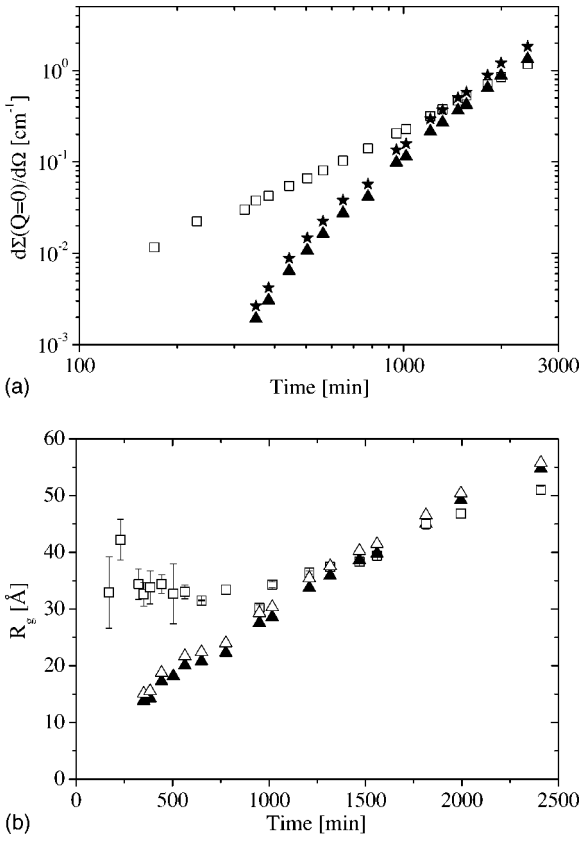

FIG. 8. Parameters for the small aggregates: (a) Forward scattering vs reaction time (t). (b) Radius of gyration R_g vs reaction time (t). Open squares (□): Fit results obtained from Guinier form factor analysis of the high Q region, Eq. (14). Filled triangles (▲): Corresponding parameters of tetramers calculated on the basis of the ^{1}H-NMR data, Eqs. (22) and (23). Open triangles (△): corresponding radius of gyration of η_{agg}-armed stars, see text. Following Ref. 41 the star symbol denotes the prediction for the 5.5 arm star.

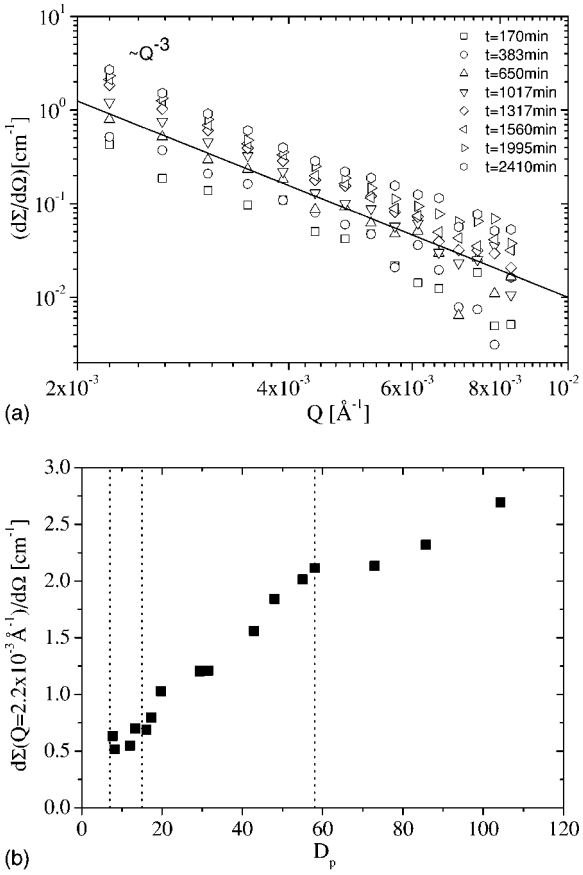

FIG. 9. (a) Time dependence of the residual power law scattering after subtraction of the Guinier form factor fit, Eq. (14). Solid line: $[d\Sigma/d\Omega] \sim Q^{-3}$. (b) Power law intensity vs degree of polymerization of the living chain; see Fig. 5.

size but rather reveals indications for the minimum size comparable with the data. Similarly, the forward scattering measured by G results in a minimum value.

Figure 9(a) shows the time dependence of the absolute scattering contribution of the large-scale aggregates at low Q. The absolute scattering intensity of these aggregates grows with reaction time and the power law $[d\Sigma/d\Omega] \sim Q^{-p}$ exists even at the beginning of the polymerization. Addressing the time dependence of the intensity growth we can relate it to chain growth in terms of $D_p(t)$ (Fig. 5). Figure 9(b) presents the power law intensity as a factor of $D_p(t)$. During initiation a linear relation holds indicating that the large-scale aggregates are built from the chains. We cannot give a precise value for the size of the large-scale aggregates (LSA) but the values of R^{LSA} obtained from a fit of the modified Beaucage form factor are reasonable estimates for the lower limit of the aggregate size. These estimates vary from a starting value of $\approx$1500 Å and reach asymptotic values $\approx$2000 Å at the end of the initiation period. The fractal dimensions are derived from the power law and yield values from $P \approx 3$ increasing to $P \approx 3.2$ with increasing reaction time.

IV. DISCUSSION

The initiation of butadiene must be viewed in terms of aggregate sizes, structures, and functionalities along with the participation of aggregates formed by cross association and the binding energies of the head groups in the various structures. Cross aggregates are recognized to form when an RLi is added to a solution of high molecular weight living polymer. Concentrated solution viscosity measurements have shown that cross aggregates are formed between *n*-, *sec*-, *t*-butyllithium or ethyllithium, and poly(isoprenyl)lithium and poly(styryl)lithium.[21,42,48–51] The results involving ethyllithium and poly(isoprenyl)lithium suggested[51] that the favored stoichiometry of the cross aggregate was $PILi(EtLi)_3$. These intermolecular exchange events reach completion within the time scale of no longer than several minutes at room temperature. Each head group of the mixed aggregates may have the capacity to react (in the aggregated state) with its own unique kinetic order and rate constant. Certainly during the early stages of the initiation reaction the mixed aggregate structures could coexist with the predominating *t*-butyllithium tetramers formed from the initiator. The stoichiometry of the mixed aggregate *t*-butyllithium allylic lithium structures would then be time dependent. Roovers and Bywater[52] have noted that for aliphatic solvents *t*-butyllithium shows sigmoidal behavior in the early stages of the initiation of isoprene and styrene. They noted that "the reaction rate increases as mixed aggregates are formed."

The generic initiation reaction, developed for aromatic solvents,[9] involves the following where $n=4$ or 6:

$$(RLi)_n \leftrightarrow nRLi. \tag{18a}$$

The singlet species were taken[9] to be the only reactive structure. A problem with this view is that the experimentally observed activation energies of initiation (18 kcal/mol) appear to be too low to account for the complete dissociation of the initiator aggregate which according to theory would require the amount to be 108 kcal/mol.[53] Clearly an imbalance exists. It is interesting to note that *t*-butyllithium shows first-order behavior in initiator for styrene and isoprene in benzene.[52]

An alternative mechanism (based on theoretical calculations[53]) involves the stepwise aggregate dissociation where the singlet *n*-butyllithium emerges:

$$(BuLi)_6 \leftrightarrow (BuLi)_4 + (BuLi)_2,$$

$$(BuLi)_2 \leftrightarrow 2BuLi, \tag{18b}$$

where the singlet organolithium then reacts with the monomer. This dissociation sequence would be expected[54] to yield a reaction order of 1/4 rather than 1/6. Brown reported[54] the mass spectrum of ethyllithium vapor ($\sim$87 °C:0.08 Hg pressure) revealed hexamers as the sole structure present. No trace of lesser aggregates or the singlet species was present. This is compelling evidence that these associated head groups must thus react directly with monomer. This conclusion is fortified by the observation that the dimeric allylic lithium head groups can show a dissociation enthalpy of $\sim$40 kcal/mol.[22,36]

As Brown[54] and Szwarc[55] have shown this value is sufficient (at room temperature) to limit the formation of sufficient singlet active centers for the propagation event to occur at a reasonable rate. Thus aggregate lifetimes are too long to allow the mechanistically required singlet head groups to be the sole reactive species. This conclusion is in concert with that of Watanabe and co-workers.[33] The finding that vitrified poly(styryl)-lithium reacts rapidly with gaseous butadiene[20] and carbon dioxide[56–58] also demonstrates that aggregated head groups are reactive entities. The sub-glass-transition temperature ($\sim$20 °C) of the polystyrene suppresses the facile head group dissociation step required by the Worsfold–Bywater mechanism.[9] The notion that aggregated head groups can react directly with monomer was independently reached by Makowski and Lynn[26] and Brown[54] in 1966. Further evidence to support this joint assessment was given in 1968 by Makowski, Lynn, and Bogard.[59,60] Others have since reached the same conclusion.[61,62] Smart *et al.* in 1974 presented[63] a mechanism for the reaction of dienes with the dimer of allylic lithium. The singlet head group played no role in this mechanism.

As we have noted the postulates upon which the Worsfold–Bywater mechanism is formulated are the dual notions that aggregated organolithium head groups lack reactivity and that the aggregation state is directly reflected in the measured kinetic order of both the initiation and propagation steps. However, the necessary agreement between reaction order and aggregation states is elusive. Parallel with these factors is the necessity of aggregate lifetimes being sufficiently short so as to release a sufficient supply of active centers so that reactions will progress at a reasonable rate. The measure[33] of these lifetimes τ shows that dissociation (at room temperature) is infrequent. This, in turn, is in consonance with the measured and calculated values of the dissociation enthalpies of the dimeric aggregates.

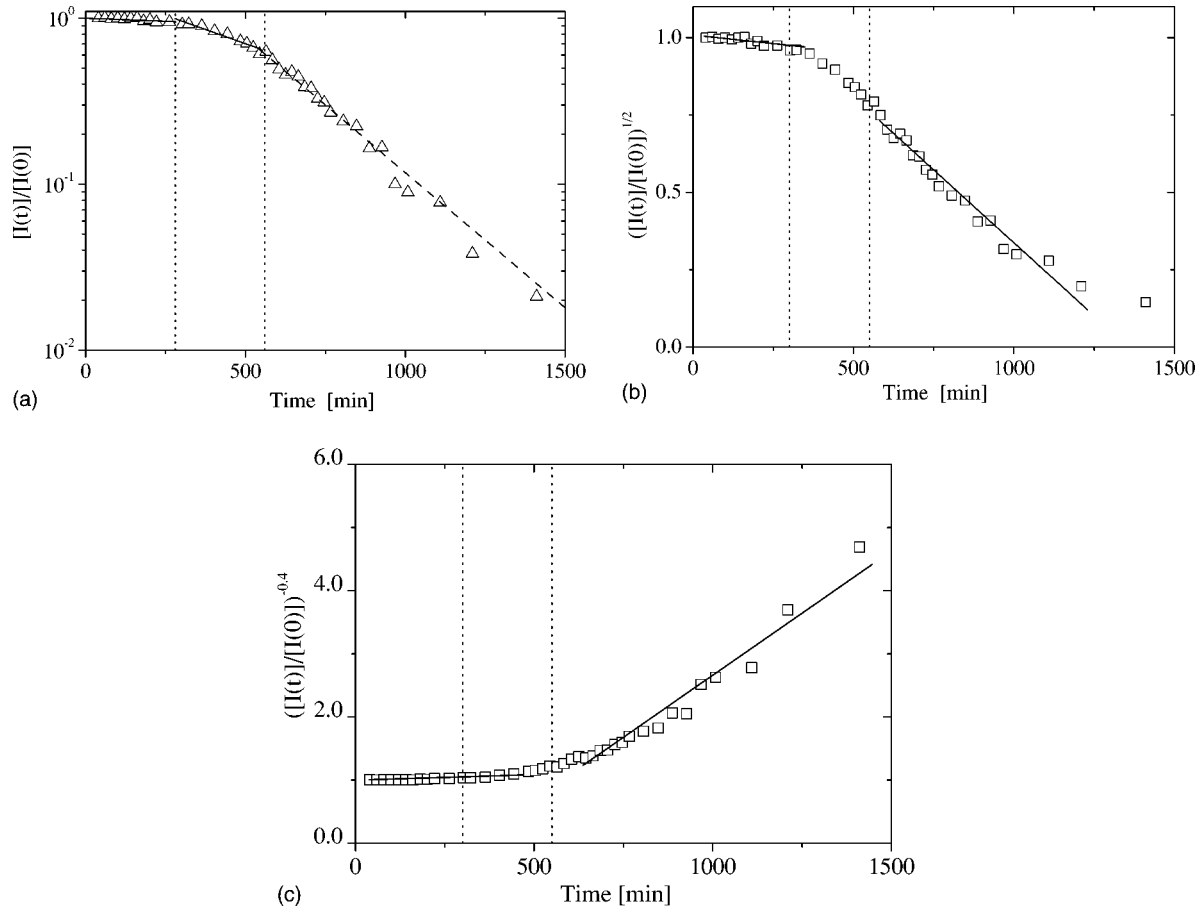

FIG. 10. Initiator concentration as a function of reaction. (a) Testing for first-order reaction (Eq. (19)). (b) Testing for a reaction order of $\frac{1}{2}$ [Eq. (20)] with $\eta_{agg}=2$. (c) Testing for a reaction order of 1.4 (see text).

A. Kinetics from NMR

The most prominent feature of anionic polymerization performed in nonpolar, aliphatic solvents is the initial slow initiation event relative to that seen in benzene and reaction orders (0.2–1.4) that are unrelated to the initiator aggregation state.[1] A system can exhibit variable initiation reaction orders at different stages of the initiation event.[48] The change of initiation rate with time, as shown in Fig. 10(a) for our system, indicates a kind of autocatalytic process in the initiation process. After the cessation of the initiation step ~10% of the monomer was consumed.[64] This corresponds to an average chain molecular weight of ~3 kg/mol (D_p ~56). This autocatalytic behavior was also seen for the system *s*-butyllithium-isoprene-cyclohexane.[50] In that instance the increase in UV absorption of the isoprenyl-lithium head group was followed to monitor the initiation reaction.

The initiation kinetics of dienes with the butyllithium isomers in aliphatic hydrocarbons is first order on monomer concentration. In analyzing our data, we took into account the possible reaction orders with respect to the initiator. This can be done by plotting the initiator concentration $[I(t)]$ versus reaction time (t) in such a way that a linear representation for the full time dependence is obtained. Assuming monomer concentration is constant during the initiation period, the integration of Eq. (5) gives:

$$\left(\frac{[I(t)]}{[I(0)]}\right) = \exp(-k_{app}t)n_{agg} = 1, \tag{19}$$

$$\left(\frac{[I(t)]}{[I(0)]}\right)^{1-(1/n_{agg})} = 1 - \left(1 - \frac{1}{n_{agg}}\right)\left[\frac{k_{app}t}{[I(0)]^{1-(1/n_{agg})}}\right], \tag{20}$$

where k_{app} is the apparent rate and k_i the initiation rate constant, $k_{app}=k_i\,[M]$.

Figure 10(a) presents the initiation behavior via the plot of $\log([I(t)]/[I(0)])$ against the reaction time. It is obvious that first-order behavior covering the whole initiation period cannot be found in our case. However, if that period is separated into three different regimes, linear relations between $[I(t)]$ and t can be found between 0–1500 min,

$$([I(t)]/[I(0)]) = \exp[(-1.7x10^{-4} \pm 1.4x10^{-5})t] \quad \text{for } 0 < t < 280 \text{ min}, \tag{21a}$$

$$([I(t)]/[I(0)]) = 1.54\ \exp\ [(-1.57x10^{-3} \pm 1.5x10^{-1})t] \quad \text{for } 280 < t < 560 \text{ min}, \tag{21b}$$

$$([I(t)]/[I(0)]) = 4.99\ \exp[(-3.75x10^{-3} \pm 1.4x10^{-1})t] \quad \text{for } 560 < t < 1500 \text{ min}. \tag{21c}$$

These regimes differ dramatically in reaction rate. Whereas at the beginning the consumption of the initiator is extremely slow, the reaction is much quicker at later stages. As values between ~0.4 and 1.4 were reported for the kinetic order of the initiator concentration in the system isoprene/*s*-butyllithium/cyclohexane[48] these values were also

considered in our analysis. Accordingly Figs. 10(b) and 10(c) show plots of $([I_t]/[I_0])^{0.5}$ versus t and $([I_t]/[I_0])^{-0.4}$ versus t. Obviously no linear relation was found for the whole initiation period. However, in both cases it was possible to divide the initiation period into two linear regimes as indicated by the solid lines. For illustration we have included the regime boundaries from Fig. 10(a). This result shows that during the initiation period at least two, and possibly three, kinetic processes take place.

Slow initiation considerably complicates a kinetic analysis of the propagation step. The number of propagating allylic active centers increases with time. The commonly used rate equations as given in the Introduction are only valid if the initiation is completed. This can be rationalized from Fig. 4(a), where the time dependence of the normalized monomer concentration during the whole polymerization period is shown. In the $\log[M(t)]/[M(t=0)]$ versus t representation no single linear regime is found as it would be expected for a first-order kinetics with respect to monomer concentration.[1] But this holds not only in the initiation period [Fig. 4(b)] but also at later reaction times when initiation is complete. During the latter period there is a clear indication that the propagation rate R_p increases at $\approx$4900 min. The average chain molecular weight M_n at this transition is $\approx$11 kg/mol. The dependence of the propagation rate upon chain length has been previously reported.[13,18,46]

Also note that at the crossover to the propagation only regime equations (11b) and (11c) are close to identical. The near independence from residual initiator $([I]_t/[I]_0=0.64$ at 560 min) of monomer consumption has not been reported previously. Thus, the analysis of only monomer concentration (dilatometry or UV spectroscopy) would lead to the false conclusion that the initiation event was finished, $t=544$ min, much earlier than its actual cessation.

B. Structural information from SANS

As mentioned above, our SANS data unambiguously reveal the presence of two different species of scattering particles.

(i) Large-scale aggregates with a characteristic size $R_g \geqslant 1500$ Å are significant during the early stages of polymerization. These large-scale aggregates have only been recently revealed[28–32] and are not at all taken into account in any of the available kinetic considerations.

(ii) Much smaller aggregates, $R_g \approx 100$ Å, which are formed in course of the polymerization.

These latter aggregates can be identified with the principal aggregates discussed in context of the commonly accepted textbook polymerization mechanism. Their size increases with time and since the mechanism assumes them to be tetramers, which resemble a four-armed star polymer, we will therefore call them starlike aggregates in the following.

We first discuss the relation between structural data obtained by SANS and kinetic data obtained from ^{1}H-NMR of the two types of aggregates separately. The formation of cross aggregates during the initiation period also influences the analysis of our SANS data. Aggregates are built from living chains only, or the aggregates consist of both types of building units, namely, living chains *and* unreacted initiator molecules. These possibilities complicate a quantitative analysis, in particular, for the large-scale aggregates. Thus, in the following we can only derive limiting estimates.

C. Small aggregates

Figure 8 shows the time dependence of the forward scattering and radius of gyration of the small aggregates obtained from a model-free Guinier analysis. We can now compare these data with the predictions made by the textbook mechanism. From the ^{1}H-NMR data we know the time dependence of the following two quantities.

(i) The degree of polymerization, $D_p(t)$, that can be used to calculate the molecular weight $M_n(t)$ of the growing chain, $M_n(t)=D_p(t)M_m+M_{ini}$ and the corresponding molecular volume $V_n(t)=M_n(t)/\rho$. Here M_m and M_{ini} are the molecular weights of the repeat unit and the initiator, respectively, and ρ is the polymer density.

(ii) The conversion $\mathrm{Conv}(t)$, from which we can calculate the total volume fraction of already reacted monomers, $\Phi_{tot}(t)=\mathrm{Conv}(t)\Phi_0$, with $\Phi_0=[M(0)/\rho]$ the initial monomer volume fraction.

From these quantities we can now calculate the expected amplitude (forward scattering) for a SANS experiment expected for a tetramer $n_{agg}=4$:

$$\left(\frac{d\Sigma}{d\Omega}(Q=0,t)\right)=\phi_{tot}(t)\frac{\Delta\rho^2}{N_A}n_{agg}V_w(t). \tag{22}$$

This quantity is also shown in Fig. 8(a). Obviously, in the early stages of the polymerization, the observed forward scattering is by far larger than the predicted tetramer scattering. Only after $\approx$1500 min, i.e., after cessation of initiation, the experimental and theoretical curves merge [Figs. 8(a) and 8(b)].

We can also calculate the radius of gyration of a starlike tetramer. For the Benoit form factor,[43] Eq. (9), the following relation between star radius of gyration and arm radius of gyration is valid:

$$R_{g,\mathrm{star}}=\sqrt{(3f-2)/f}\,R_{g,\mathrm{arm}}. \tag{23}$$

The arm radius of gyration can be estimated from the scaling relation between R_g and M_w, $R_g(t)=a\,M_w^{\nu}(t)$. To be as precise as possible we investigated (via SANS) a series of low molecular weight poly(butadienes), with $500 \leqslant M_w \leqslant 8000$ g/mol in *d*-heptane and obtained the following:

$$R_g=0.288\,M_W^{0.554}. \tag{24}$$

The calculated $R_{g,star}(t)$ is compared to the experimental data in Fig. 8(b). As already observed for the forward scattering, we found that the experimental $R_g(t)$ is by far larger than the theoretical prediction for tetramers during the first 1500 min, i.e., during the initiation period.

We can therefore unambiguously conclude that during the initiation period starlike tetramers from the allylic head

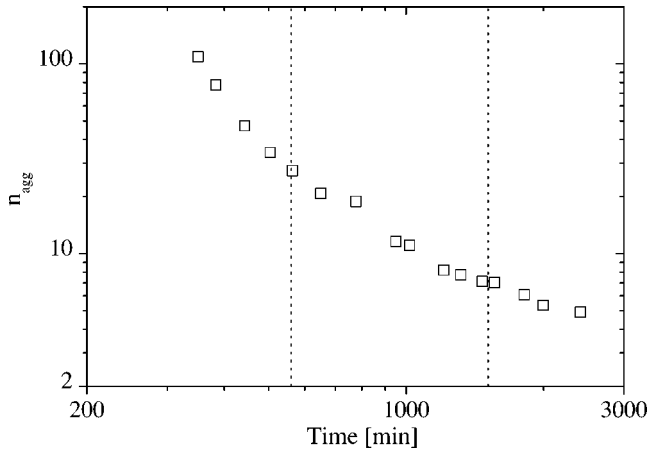

FIG. 11. Aggregation number n_{agg} of small and starlike aggregates calculated by combining *in situ* SANS and ^{1}H-NMR results using Eq. (22) vs reaction time (t). Dashed lines represent the divisions between the different regimes; see Eq. (11).

groups are not present since they cannot explain n either the SANS data regarding the forward scattering n or the radius of gyration results.

From the experimental forward scattering we can estimate the aggregation number $n_{agg}(t)$ simply by use of Eq. (22) since all other parameters are known or given by experiment. Figure 11 (log–log) shows the time dependence of n_{agg}. We found surprisingly high values for $n_{agg} \approx 100$ at early times in the initiation period, which reach the limit of ≈ 5 during the period of pure propagation. This decrease in aggregation state is also encountered in the Makowski and Lynn[26] data of melt state oligomeric butadienyllithium.

The growth of the chain thus can cause a concurrent decrease in aggregate functionality. Comparison of Fig. 10(a) and Fig. 11 shows that the increasing initiation rate is reflected in the decrease of the aggregation number. During the initial period of initiation, the initiation rate is very slow and living polymer chains appear with high aggregation numbers only at ~ 350 min. The corresponding D_p is ~ 7. Thereafter, the aggregation decreases dramatically from ~ 100 by the end of the second regime [Eq. (21)]. The initiation rate constant is ~ 10 times higher than the first regime and the corresponding D_p of living chains grow from ~ 7 to ~ 13. In the third regime of initiation, the aggregation number of living chains decrease slowly and level off at $n_{agg} \sim 5$. Both aggregation states and initiation rates change with reaction time.

Assuming a starlike architecture of the aggregates we can calculate their radius of gyration $R_{g,star}(t)$ as described above, but now using $n_{agg}(t)$ instead of the constant value of 4. These data are also shown in Fig. 8(b), but again, during the initiation period, are found to be much smaller than the experimental values. In addition, a starlike architecture built by chains with such an extremely small $D_p \sim 10$, and a large aggregation number, is very unlikely. Unfortunately, the detailed molecular architecture of the aggregates during the initiation period cannot be determined from our SANS data, because at early times the data quality is insufficient. Thus we are restricted to the Guinier regime of these small particles.

In analogy to short chain surfactants we may assume that the highly aggregated small D_p living chains form wormlike aggregates. This was proposed by Frischknecht and Milner.[36] The following estimate can be made. The end-to-end distance of the wormlike chain can be calculated from the experimentally found R_g by $R_e = \sqrt{6}\, R_g \approx 86$ Å at $t < 1000$ minutes (where R_e is the chain end-to-end distance). The corresponding persistence length l can be estimated by $R_e = l^2 n$, where n is given by $n_{agg}/2$ due to dimerization. We obtain $l \approx 86\ \text{Å}/\sqrt{50} \approx 12.2$ Å, which transforms into 4–6 Li–Li bonds along the persistence length of the wormlike chain.

In the Frischknecht–Milner[36] calculation at low D_p an equilibrium between wormlike chains and starlike aggregates was found. From their calculations at $D_p \geqslant 26$ the equilibrium is strongly in favor of the star mode. From Fig. 8(a) the predicted[36] forward scattering for stars with an average aggregation number of 5.5 merges with the observed behavior at $t = 1200$ min. corresponding to the $D_p = 43$. Thus in the real system the equilibrium appears to be shifted to somewhat higher D_p.

In all the calculations given above we assumed that only the living polymer chains are the building blocks of the aggregates, i.e., we neglected any kind of cross association. The general effect of initiator molecules participating in the aggregates would be to increase n_{agg}, the number of building blocks in the aggregate. In the forward scattering this contribution would be small since the molecular weight of the initiator *t*-butyllithium is much smaller (approximately those of a monomer unit), than that of the living polymer chains, see Eq. (22).

Moreover, we also assumed that all living chains are participating in the starlike aggregates only, i.e., we neglected the presence of the large-scale aggregates. Also a partitioning of the living chains between both types of aggregates would have the effect of increasing the aggregation number $n_{agg}(t)$ since the volume fraction would now be smaller than Φ_{tot}, see Eq. (22). Our conclusion, that the small aggregates have aggregation numbers much larger than the predicted value of 4 and are not starlike during the initiation period, can only be confirmed by taking into account the two aforementioned effects.

D. Large-scale aggregates

In our previous work,[30] a power law with $P \approx 3$ was found from the scattering contribution of the large scale aggregates at low Q range in styryllithium benzene solutions, and the slope P was independent of polymer concentration. The measured fractal dimension of $P \approx 3$ indicates aggregated objects the mass of which grows with the spatial dimension to the power 3. Also the fact that the intensity grows in proportion to D_p [Fig. 9(b)] supports the Frischknecht–Milner picture[36] of aggregates constructed from linear chains.

In previous publications[29–32] we estimated that the amount of living polymer chains contributing to the large-scale aggregates is only a very minor fraction $\leqslant 1\%$. This can be estimated from the amplitude G of the Beaucage form factor [Eq. (16)] for fitting the SANS data. From the fractal

dimension $P=3$, we can estimate their aggregation number in terms of subunits by $n_{agg}^{\mathrm{LSA}}(t)=(R^{\mathrm{LSA}}(t)/R_{\mathrm{sub}}(t))^3$. Assuming that the radius of the large-scale aggregates R^{LSA} is $\approx$1500 Å as obtained from the Beaucage form factor fit, the crucial point in determining n_{agg}^{LSA} is, which value we have to use for R_{sub}, the size of the subunits of the large scale aggregates. Here three different approaches can be made, which are as follows.

(i) The large-scale aggregates are directly built from dimers of the living chains, i.e., we have to use their radius of gyration calculated on basis of the ^{1}H-NMR data. At early reaction times we calculated a value of $\approx$13 Å for the dimers and so we obtain $n_{agg}^{\mathrm{LSA}}\approx 2\times 10^6$.

(ii) The building blocks of the large-scale aggregates are the small aggregates, i.e., we have to use their radii of gyration as determined by SANS. At early polymerization times we found a value of $\approx$35 Å and so we obtain $n_{agg}^{\mathrm{LSA}}\approx 8\times 10^4$.

(iii) Another way to estimate n_{agg}^{LSA} without any assumption is, to use the lower and upper limits $Q_{\mathrm{min}}=2.2\times 10^{-3}$ Å^{-1} and $Q_{\mathrm{max}}=1\times 10^{-2}$ Å^{-1} in between the power law behavior is observed in our SANS data. This is valid for any type of structure of the large-scale aggregates and its subunits. So we do not even have to know the precise values of R^{LSA} and R_{sub}. All we use is the ratio $[Q_{\mathrm{max}}/Q_{\mathrm{min}}]\approx 5$ since we know that R^{LSA} must be larger than $1/Q_{\mathrm{min}}$ and that R_{sub} must be smaller than $1/Q_{\mathrm{max}}$. Therefore we can estimate $n_{agg}^{LSA}=[Q_{\mathrm{max}}/Q_{\mathrm{min}}]^3\approx 10^2$.

We wish to emphasize that the reader should not interpret this large variation in the estimated values of $n_{agg}^{LSA}(t)$ as a measure of uncertainty of our experiments. It results from the already different aggregation states of the subunits, i.e., the building blocks of the large-scale aggregates, given by their own aggregation number n_{sub}. The only important quantity is the total aggregation number in terms of single living chains $n_{agg}^{LSA}(t)$ which is just the product of $n_{agg}^{LSA}(t)$ and n_{sub}. For the scenarios given above we have to use for case (i) $n_{\mathrm{sub}}=2$ and for case (ii) $n_{\mathrm{sub}}=n_{\mathrm{agg}}\approx 100$. To estimate n_{sub} for case (iii) we now make the assumption that the subunits have the same wormlike chain architecture as the small aggregates during the early stages of initiation, see above. Then we can use the estimated persistence length and we finally obtain $n_{\mathrm{sub}}=[R_{sub}/R_g]^2[n_{agg}/2]$. The crucial point now is to estimate a value for R_{sub}. Since we are starting in this case from the ratio of the observed limits of the power law regime in Q, $[Q_{\mathrm{max}}/Q_{\mathrm{min}}]\approx 5$, a reasonable value for R_{sub} is $R^{\mathrm{LSA}}/5=300$ Å. This gives finally $n_{\mathrm{sub}}\approx 5\times 10^3$ for case (iii). Therefore $n_{agg}^{LSA}(t)$ turns out as follows for the three assumed scenarios, (i) $n_{\mathrm{total}}^{\mathrm{LSA}}(t)\approx 3\times 10^6$, (ii) $n_{\mathrm{total}}^{\mathrm{LSA}}(t)\approx 9\times 10^6$, and (iii) $n_{\mathrm{total}}^{\mathrm{LSA}}(t)\approx 5\times 10^5$. In combination with the molecular volume of the growing polymer chain obtained from the ^{1}H-NMR data, $V_w(t)=[D_p(t)M_m+M_{ini}]/\rho$, we can then calculate by simply using $V^{\mathrm{LSA}}(t)=n_{\mathrm{total}}^{\mathrm{LSA}}(t)V_{\mathrm{w}}(t)$.

The next step is to calculate the volume fraction of monomers building up the large-scale aggregates, which is obtained by $\Phi^{LSA}(t)=[G(t)/V^{LSA}(t)]N_A/\Delta\rho^2$. Since the fit of the forward scattering resulting from the large-scale aggregates gives parameters with extremely large error bars, see Sec. III C, we decided to use the value of the first data point, $I(Q=2.2\times 10^{-3}t)$ to estimate $\Phi^{LSA}(t)$. Finally we can calculate the relative volume fraction x^{LSA} of reacted monomers present in the large-scale aggregates by $x^{LSA}=\Phi^{LSA}(t)/\Phi_{tot}(t)$. This results in values between 5×10^{-4} and 3×10^{-3}.

We note that the large-scale aggregates appear to be formed by living chains [Fig. 9(b)]. The thermodynamic reason for their formation is not at all clear. It is very difficult to understand why such a small fraction of living chains should form these large-scale structures. There may also be a kinetic reason. Following initiation the newly created neopentylallyllithium (the $\sim$1/1 adduct of butadiene and *t*-butyllithium) forms a gel-like paste at high concentration.[65] Under polymerization conditions a fraction of these highly aggregated structures may not completely dissolve and thus in someway becomes kinetically arrested. Further research is needed.

V. CONCLUSIONS

In this work for the first time *in situ* measurements of an anionic polymerization, both in the initiation and propagation phase, were performed combining structural data (SANS) and kinetic data (^{1}H-NMR). In this way independent results on the detailed kinetics could be related to information about structure formation in terms of aggregate functionalities. It is clear that the measurement of kinetic orders is not a tool that can be used to assay aggregation states as has long been assumed.

Thus, kinetics and aggregation states were investigated under standard polymerization conditions and not by using postpolymerization measurements or "artificial" reaction conditions (high initiator concentrations or low monomer/initiator ratios). The latter is a characteristic of the propagation and initiation studies that were conducted using UV-visible spectrometry as the investigative tool.[9,39,40,49,50] This *in situ* study has shown that the initiation and propagation events involving an organolithium initiator and butadiene are more complicated than previously envisioned. Following commencement of initiation ($\sim$1% monomer consumption) SANS detected the large-scale structures and the high functionality smaller pre-star-shaped aggregates. As initiation and propagation proceded these initially small structures simultaneously increased in size while undergoing a decrease in average functionality. The star-shaped architecture becomes detectable as the polymerization progresses (at a $D_{\mathrm{p}}\approx 40$). In the early reaction stages where initiation and propagation occur simultaneously the dominating structures appear to be wormlike. The limiting mean value of $n_{agg}\sim 5$ was found for the star-shaped structures of high D_{p}.

The period when initiation and propagation occurred simultaneously was found to consist of three regimes where the initiation rate increased with time. Concurrently, the monomer consumption rate was found to increase. In parallel the aggregation states of the living chains are decreasing with increasing rate. Furthermore an increase of the monomer consumption rate was found to also occur during the

postinitiation period. This feature has been previously observed.[13,18,46] The presence of residual *t*-butyllithium leads to an increase in 1, 2 content of the chain relative to what is obtained ($\approx$6%) when initiator is depleted.[26,35]

This general behavior can be viewed within the context of the existence of active cross aggregates formed from initiator and the poly(butadienyl)lithium head groups. In this scenario it was found that the aggregates of *t*-butyllithium are initially highly unreactive leading to a very small initiation rate at the beginning of the process (0–280 min). With ongoing reaction the polymer chain head groups form cross aggregates with *t*-butyllithium. In that format the initiator becomes much more reactive than in the pure self-aggregated state. At the 280 min crossover $\sim$1% of the initiator has reacted. For $>$560 min ($\sim$34% initiator usage) the initiation reaction rate is constant until the *t*-butyllithium concentration approaches zero. It should be noted that ^{7}Li-NMR (Ref. 66) and ^{13}C-NMR (Ref. 67) based data has been interpreted as showing the coexistence of aggregates with varying functionalities in solutions of oligomeric isoprenyllithium and butadienyllithium.

We wish to emphasize that the combination of NMR and SANS has allowed new insight into the relation between structure formation and chemical kinetics in these anionic systems. This provided information that could not be obtained by the sole application of the usual kinetic techniques. We will use this approach for a detailed analysis of the reaction kinetics and structure formation with respect to varying initiator concentration.

[1] H. L. Hsieh and R. P. Quirk, *Anionic Polymerization* (Marcel Dekker, New York, 1996), see Tables 6.1 and 6.2 for a listing of organolithium aggregation states and initiation reaction orders.
[2] G. Frankel, W. E. Beckenbaugh, and P. P. Yang, J. Am. Chem. Soc. **98**, 6878 (1976).
[3] E. Weiss, Angew. Chem. **32**, 1501 (1993).
[4] M. Szwarc and M. Van Beylen, *Ionic Polymerization and Living Polymers* (Chapman and Hall, New York, 1993).
[5] M. Szwarc, Adv. Polym. Sci. **49**, 1 (1983).
[6] R. N. Young, R. P. Quirk, and L. J. Fetters, Adv. Polym. Sci. **56**, 1 (1984).
[7] M. Van Beylen, S. Bywater, G. Smets, M. Szwarc, and D. J. Worsfold, Adv. Polym. Sci. **92**, 1236 (1988).
[8] M. Szwarc, *Ionic Polymerization Fundamentals* (Hanser, New York, 1996).
[9] D. J. Worsfold and S. Bywater, Can. J. Chem. **38**, 1891 (1960).
[10] Y. L. Spirin, A. R. Gantmakher, and S. S. Medvedev, Dokl. Akad. Nauk SSSR **146**, 368 (1962).
[11] G. Geerts, M. Van Beylen, and M. Smets, J. Polym. Sci. [A1] **7**, 2859 (1969).
[12] R. Ohlinger and F. Bandermann, Makromol. Chem. **181**, 1935 (1980).
[13] A. Maliakal, H. Greenaway, B. O'Shaughnessy, and N. J. Turro, Macromolecules **36**, 6075 (2003).
[14] L. J. Fetters, J. S. Huang, and R. N. Young, J. Polym. Sci., Part A: Polym. Chem. **34**, 117 (1996).
[15] A. F. Johnson and D. J. Worsfold, J. Polym. Sci. A **3**, 449 (1965).
[16] D. J. Worsfold, J. Polym. Sci. A **5**, 2783 (1967).
[17] D. J. Worsfold and S. Bywater, Can. J. Chem. **42**, 2884 (1964).
[18] S. Bywater and D. J. Worsfold, in *Recent Advances in Anionic Polymerization*, edited by T. Hogen-Esch and J. Smid (Elsevier, New York, 1987).
[19] D. J. Worsfold and S. Bywater, Macromolecules **5**, 393 (1972).
[20] R. N. Young, L. J. Fetters, J. S. Huang, and R. Krishnamoorti, Polym. Int. **5**, 217 (1994).
[21] M. Morton, E. Bostick, and R. A. Livigni, Rubber and Plastics Age **42**, 397 (1961).
[22] M. Morton and L. J. Fetters, J. Polym. Sci. A **2**, 3311 (1964).
[23] L. J. Fetters and M. Morton, Macromolecules **7**, 552 (1974).
[24] M. M. Al-Jarrah and R. N. Young, Polymer **21**, 119 (1980).
[25] M. Morton, L. J. Fetters, R. A. Pett, and J. Meier, Macromolecules **3**, 237 (1970).
[26] H. Makowski and M. Lynn, J. Macromol. Sci., Chem. **1**, 443 (1966).
[27] A. Hernandez, H. C. Semel, H. C. Broacher, H. C. Zachmann, and H. Sinn, Makromol. Chem., Rapid Commun. **1**, 75 (1980).
[28] L. J. Fetters, N. P. Balsara, J. S. Huang, H. S. Jeon, K. Almdal, and M. Y. Lin, Macromolecules **28**, 4996 (1995).
[29] J. Stellbrink, L. Willner, O. Jucknischke, D. Richter, P. Lindner, L. J. Fetters, and J. S. Huang, Macromolecules **31**, 4189 (1998).
[30] J. Stellbrink, L. Wilner, D. Richter, P. Lindner, L. J. Fetters, and J. S. Huang, Macromolecules **32**, 5321 (1999).
[31] J. Stellbrink, J. Allgaier, L. Wilner, D. Richter, T. Slawecki, and L. J. Fetters, Polymer **43**, 7101 (2002).
[32] A. Niu, J. Stellbrink, J. Allgaier *et al.*, Macromol. Symp. **215**, 1 (2004).
[33] H. Y. Watanabe, T. Kanaya, H. Kaji, and F. Horii, Macromolecules **36**, 220 (2003).
[34] R_g denotes the single chain or aggregate radius of gyration.
[35] S. Bywater, Macromolecules **31**, 6010 (1988).
[36] A. L. Frischknecht and S. T. Milner, J. Chem. Phys. **114**, 1032 (2001).
[37] M. Morton and L. J. Fetters, Rubber Chem. Technol. **48**, 359 (1975).
[38] The use of calcium hydride as a drying agent is common for monomers and solvents. We experienced an undesirable event when dry and used calcium hydride was disposed of. The hydride had been used for $\sim$2 weeks for drying solvent. Following solvent removal (via distillation) the dry flask was removed from the vacuum line. Methanol was added at room temperature to decompose the residual calcium hydride. This led to the prompt ignition of the methanol. This is abnormal behavior. The ignition event, we believe, was caused by the presence of fine iron filings from the Teflon® coated stir bar which was observed to have developed a bare spot. This abrasion took place during the two week span of stirring the granular contents of the flask.
[39] J. E. L. Roovers and S. Bywater, Trans. Faraday Soc. **62**, 1876 (1966).
[40] J. E. L. Roovers and S. Bywater, Macromolecules **1**, 328 (1968).
[41] H. L. Hsieh, J. Polym. Sci. [A1] **8**, 533 (1970).
[42] A. Guyot and A. Vialle, J. Macromol. Sci., Chem. **A4**, 107 (1977).
[43] T. L. Brown, J. L. Ladd, and G. N. Newman, J. Organomet. Chem. **3**, 1 (1965).
[44] H. Benoît, J. Polym. Sci. **11**, 507 (1953).
[45] J. S. Higgins and H. C. Benoit, *Polymers and Neutron Scattering* (Oxford University Press, Oxford, 1994).
[46] E. Madani, J. C. Favier, P. Hémery, and P. Sigwalt, Makromol. Chem., Rapid Commun. **70**, 329 (1990). This work used α,ω-dilithio-1,4-polyisoprene chains as the "initiator." As the oligomeric polyisoprene chain length increased the propagation rate increased while the apparent propagation kinetic order was incrementally transformed from first power to $\sim 1/4$.
[47] G. Beaucage and D. Schaefer, J. Non-Cryst. Solids **172–174**, 797 (1994).
[48] S. Bywater and D. J. Worsfold, J. Organomet. Chem. **1**, 10 (1967).
[49] J. E. L. Roovers and S. Bywater, Macromolecules **5**, 328 (1972).
[50] F. Schué and S. Bywater, Macromolecules **2**, 458 (1969).
[51] M. Morton, R. A. Pett, and L. J. Fetters, Macromolecules **3**, 333 (1970).
[52] J. E. L. Roovers and S. Bywater, Macromolecules **8**, 251 (1975).
[53] G. Graham, S. Richtsmeier, and S. Dixon, J. Am. Chem. Soc. **102**, 5759 (1980).
[54] T. L. Brown, J. Organomet. Chem. **5**, 191 (1966).
[55] M. Szwarc, J. Polym. Sci., Polym. Lett. Ed. **18**, 493 (1980).
[56] R. P. Quirk and W.-C. Chen, Makromol. Chem. **183**, 2071 (1982).
[57] R. P. Quirk, J. Yin, and L. J. Fetters, Macromolecules **22**, 85 (1989).
[58] R. P. Quirk, J. Yin, L. J. Fetters, and R. V. Kastrup, Macromolecules **25**, 2262 (1992).
[59] H. Makowski and M. Lynn, J. Makromol. Sci. Chem. **2**, 683 (1968).
[60] H. Makowski, M. Lynn, and A. N. Bogard, J. Makromol. Sci. Chem. **2**, 665 (1968).
[61] P. v. R. Schleyer, Pure Appl. Chem. **56**, 151 (1984).
[62] A. M. Sapse, D. C. Jain, and K. Raghavashari, in *Lithium Chemistry: A Theoretical and Experimental Overview*, edited by A. M. Sapse and P. V. R. Schleyer (Wiley, New York, 1995), p. 45.
[63] J. B. Smart, R. Hogan, P. A. Scheer, M. T. Emerson, and J. P. Oliver, J. Organomet. Chem. **64**, 1 (1974).
[64] H. L. Hsieh, J. Polym. Sci. A **3**, 163 (1965). This work reports that the

t-butyllithium/cyclohexane/butadiene/50 °C system reached complete initiator consumption at ~10% monomer consumption. That is identical to what was found in our work.
[65]S. Bywater, D. J. Worsfold, and G. Hollingsworth, Macromolecules **5**, 389 (1972).
[66]J.-M. Boutillier, J.-C. Favier, P. Hémery, and P. Sigwalt, Polymer **37**, 5197 (1996).
[67]A. F. Halasa, V. D. Mochel, and G. Fraenkelin, in *Anionic Polymerization: Kinetics, Mechanisms and Synthesis*, ACS Symposium Series Vol. 166, edited by J. E. McGrath (Washington, DC, 1981) p. 347.